AGU PUBLICATIONS

Geophysical Research Letters

RESEARCH LETTER
10.1002/2014GL060280

Key Points:
- Present ARTEMIS observations of extreme diamagnetic fields in the lunar wake
- Extreme diamagnetic fields are a result of high ambient plasma beta (>10)
- Successfully compare to a hybrid plasma model of the lunar wake for high beta

Correspondence to:
A. R. Poppe,
poppe@ssl.berkeley.edu

Citation:
Poppe, A. R., S. Fatemi, J. S. Halekas, M. Holmström, and G. T. Delory (2014), ARTEMIS observations of extreme diamagnetic fields in the lunar wake, *Geophys. Res. Lett.*, *41*, doi:10.1002/2014GL060280.

Received 18 APR 2014
Accepted 28 MAY 2014
Accepted article online 1 JUN 2014

ARTEMIS observations of extreme diamagnetic fields in the lunar wake

A. R. Poppe[1,2], S. Fatemi[3,4], J. S. Halekas[1,2], M. Holmström[3], and G. T. Delory[1,2]

[1]Space Sciences Laboratory, University of California, Berkeley, California, USA, [2]Solar System Exploration Research Virtual Institute, NASA Ames Research Center, Moffett Field, California, USA, [3]Swedish Institute of Space Physics, Kiruna, Sweden, [4]Department of Computer Science, Electrical, and Space Engineering, Luleå University of Technology, Luleå, Sweden

Abstract We present two Acceleration, Reconnection, Turbulence, and Electrodynamics of the Moon's Interaction with the Sun (ARTEMIS) observations of diamagnetic fields in the lunar wake at strengths exceeding twice the ambient magnetic field during high plasma beta conditions. The first observation was 350 km from the lunar surface while the Moon was located in the terrestrial magnetosheath with elevated particle temperatures. The second observation was in the solar wind ranging from 500 to 2000 km downstream, with a relatively low magnetic field strength of approximately 1.6 nT. In both cases, the plasma beta exceeded 10. We discuss the observations and compare the data to hybrid plasma simulations in order to validate the model under such extreme conditions and to elucidate the global structure of the lunar wake during these observations. The extreme nature of the diamagnetic field in the lunar wake provides an important end-member test case for theoretical and modeling studies of the various plasma processes operating in the lunar wake.

1. Introduction

As the moon absorbs solar wind plasma, it generates a plasma void downstream with steep particle density gradients along the wake boundary. These density gradients generate diamagnetic currents which in turn perturb the convecting interplanetary magnetic field. While the strength and structure of lunar diamagnetic fields depend on the plasma and interplanetary magnetic field (IMF) conditions, they typically depress the field near the outer boundary of the wake while enhancing the field inside the plasma void. Observations of diamagnetic fields in the lunar wake were first made by the Explorer 35 spacecraft [*Colburn et al.*, 1967; *Ness et al.*, 1968; *Ogilvie and Ness*, 1969], followed later by WIND [*Owen et al.*, 1996], Lunar Prospector [*Halekas et al.*, 2005], and the Acceleration, Reconnection, Turbulence, and Electrodynamics of the Moon's Interaction with the Sun (ARTEMIS) mission [*Halekas et al.*, 2011, 2014; *Zhang et al.*, 2012]. Smaller signatures of diamagnetic fields have also been observed at the moons of Saturn [*Khurana et al.*, 2008; *Simon et al.*, 2012], despite significantly different values in ambient plasma parameters (i.e., total plasma $\beta_{tot} = \beta_e + \beta_i \approx 5 \times 10^{-3} - 0.5$ at the outer planet moons versus $\beta \approx 0.1 - 10$ for the Moon). Early statistical studies of field strengths in the lunar wake at 1–2 R_L downstream for cases where $\beta < 0.7$ have shown at most a factor of 50% diamagnetic increase roughly linearly dependent on the value of plasma beta [*Ogilvie and Ness*, 1969].

Alongside in situ observations, plasma modeling has also helped to elucidate the global structure of lunar diamagnetic currents and fields and their dependence on solar wind plasma and IMF parameters. Using hybrid modeling results from *Holmström et al.* [2012], *Fatemi et al.* [2013] investigated the dependence of the lunar wake current system on the angle between the solar wind flow velocity and the IMF. For parallel flow and field, the current systems (which include the diamagnetic current and the rarefaction and recompression currents) close cylindrically around the lunar wake, while for perpendicular flow and field, all three currents couple together to close both near to the Moon and presumably, far ($\gg 10\ R_L$) downstream. Several other models have also investigated the global structure of the lunar wake, including the diamagnetic fields, often compared to the sole observation of the Wind spacecraft at approximately 6.5 R_L downstream from the Moon [*Owen et al.*, 1996; *Kallio*, 2005; *Trávniček et al.*, 2005; *Xie et al.*, 2012], while more recent modeling, both hybrid and theoretical, have also been compared to ARTEMIS observations [*Wiehle et al.*, 2011; *Halekas et al.*, 2011, 2014]. Given the complexity of the lunar wake and the wide range of ambient parameters that may affect diamagnetic currents and fields, it is important to describe further observations that may aid in

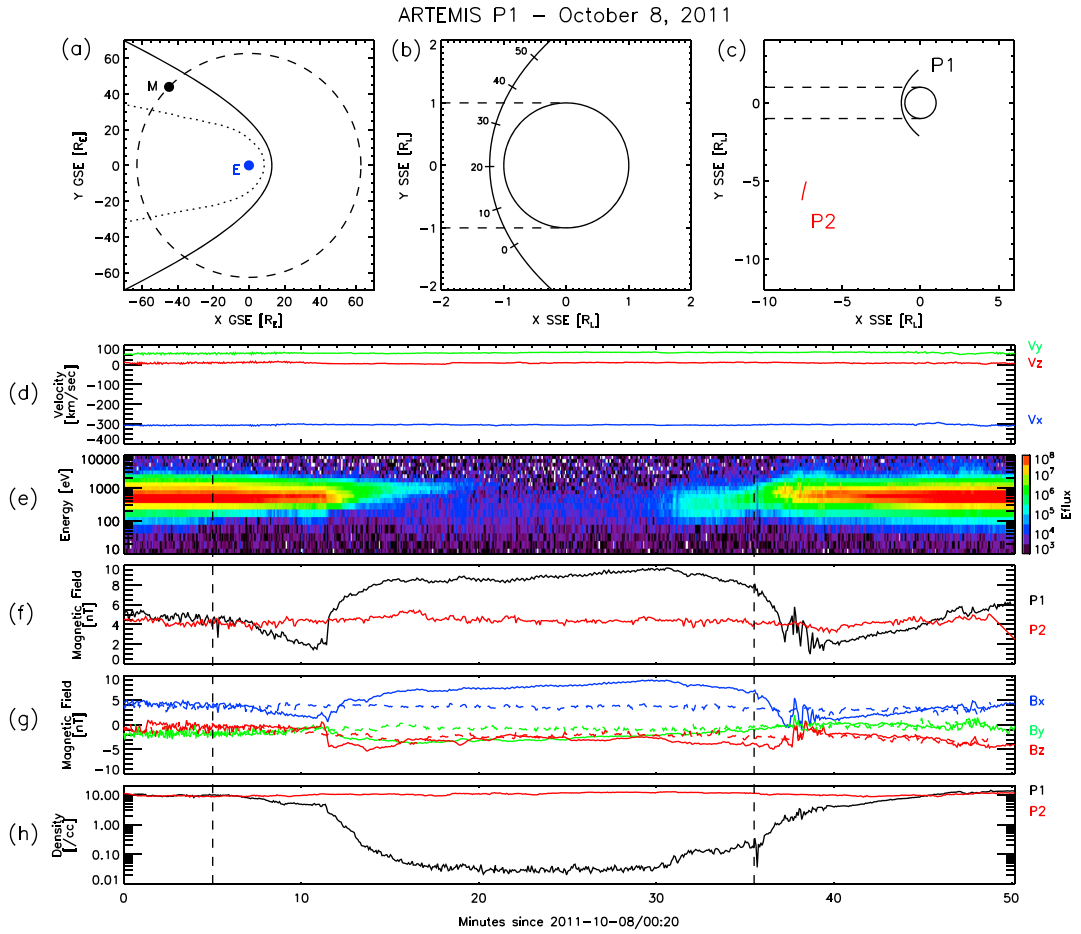

Figure 1. A time series of ARTEMIS P1 measurements on 8 October 2011: (a) the lunar position relative to the Earth and its magnetosphere during this time period in the GSE coordinate system, (b) the ARTEMIS orbit relative to the Moon in the Selenocentric Solar Ecliptic (SSE) coordinate system, with tickmarks indicating minutes past 2011-10-08/00:20 UTC along the orbit, (c) the ARTEMIS P1 and P2 orbits zoomed out, showing P2 far from the Moon, (d–h) the ambient magnetosheath flow velocity, ion differential energy flux, magnetic field magnitude for P1 in the wake (black) and P2 far from the moon (red), magnetic field components of both probes (wake in solid, reference in dashed lines), and ion density in the wake (black) and far from the Moon (red), respectively. Energy flux is measured in units of eV/cm^2/s/str/eV. The vertical dashed lines in Figure 1e–1h denote the time of the lunar optical shadow crossing, for reference.

the design, testing, and validation of various plasma models of the lunar wake. Study of such observations and accompanying modeling will also help to elucidate the underlying physical processes governing the lunar wake.

In this paper, we report two ARTEMIS observations of lunar diamagnetic fields in the wake exceeding twice the ambient magnetic field strength, far higher than any reported to date. In both observations, the plasma beta was significantly higher than normal, albeit for different reasons (high particle pressure in the first case and low magnetic pressure in the second). In section 2, we describe and discuss the ARTEMIS observations. In section 3, we describe the results of a hybrid plasma simulation of the lunar wake with parameters matching one of the ARTEMIS observations and compare the model results to the data. Finally, we conclude in section 4.

2. ARTEMIS Observations

The ARTEMIS mission consists of two identical probes, P1 and P2, in elliptical, approximately 28 h orbits around the Moon [*Angelopoulos*, 2011]. Both probes make comprehensive measurements of the ambient particle and field conditions at high time resolution. For nearly all lunar wake crossings, one probe is in the lunar wake while the other is far from both the wake and the lunar surface providing reference

Table 1. Plasma Parameters During the ARTEMIS Wake Crossings and the Hybrid Model[a]

Parameter	8 October 2011 (ART)	8 October 2011 (Model)	13 March 2013 (ART)
Solar wind velocity (km/s)	[−305, 45, 5]	[−307, 0, 0]	[−320, 15, 0]
Solar wind density (cm^{-3})	10.4	10.4	7
Magnetic field (nT)	[3.6, −1.0, −2.0]	[3.68, 2.23, 0]	[−1.5, 0, −1]
T_e, T_i (eV)	10, ≈35–45	10, (35, 39, 43)	9, ≈4–6
v_A (km/s)	29	29	14.8
M_A	10.6	10.6	21.5
c_s (km/s)	≈69	69	≈37
M_s	4.5	4.5	8.7
β_e, β_i, β_{tot}	2.3, ≈8–10, ≈10–12	2.3, 9, 11	7.8, ≈3.5–5, ≈11.5–13

[a]For the model parameters, the solar wind velocity and magnetic field have been rotated from the ARTEMIS SSE frame into the flow-aligned, planar-magnetic field coordinate system as described in section 3. Derived plasma parameters for the model have been listed for the intermediate, $T_i = 39$ eV case.

measurements of the undisturbed solar wind. Among the numerous ARTEMIS wake crossings (more than one thousand to date), the following observations were chosen due to both the large diamagnetic fields observed in the wake and the relatively steady ambient plasma conditions.

2.1. The 8 October 2011 Observation

Figure 1 shows an ARTEMIS P1 observation on 8 October 2011. During this time, the Moon was located at approximately [−44.8, 44.0, 5.3] R_E in the GSE coordinate frame and was immersed in the dusk flank of the terrestrial magnetosheath, Figure 1a. Table 1 lists the relevant ambient plasma parameters for this time period taken from the ARTEMIS P2 reference observations of the magnetosheath, with the important note that the ion temperature is only roughly measured by ARTEMIS due to the finite resolution of the ESA instrument and thus, parameters dependent on T_i are subject to some uncertainty [*McFadden et al.*, 2008]. The magnetosheath plasma at this time is both super-Alfvénic and supersonic with Mach numbers of approximately 10.6 and 4.5, respectively. The electron and ion plasma beta are elevated during this interval at approximately 2.3 and 8–10, respectively, driven mainly by the high density and high ion temperature although the somewhat low magnetic field magnitude of approximately 4 nT also contributes.

As shown in Figure 1b, for approximately 50 min following 2011-10-08/00:20 UTC, the ARTEMIS P1 probe crossed through the lunar wake with a periselene of approximately 390 km (≈ 0.23 R_L) near local midnight while the ARTEMIS P2 probe was more than 8 R_L from the Moon and free of lunar effects, shown in Figure 1c. The magnetosheath flow speed during this observation is partially deflected at approximately v_i = [−305, 45, 5] km/s in the SSE coordinate frame, Figure 1d, which accounts for the offset between the optical shadow of the Moon (dashed lines in Figures 1e–1h) and the observed plasma wake. The density and magnetic field through the wake show several features characteristic of most lunar wake crossings, including rarefaction regions near the wake edges where both the magnetic field and density decrease into the wake (approximately 5 to 11 min and 40 to 50 min, respectively), a deep plasma void with densities more than 2 orders of magnitude lower than the ambient solar wind density, and a corresponding increase and slight rotation of the magnetic field within the void (approximately 11 to 40 min). As the undisturbed IMF is B_x dominant at [3.6, −1, −2] nT, the main diamagnetic field increase occurs along the x component, with maximum values of 8 nT, or more than 200% of the ambient value. Smaller perturbations are also present in the B_y and B_z components. Overall, the magnetic field magnitude reaches nearly 10 nT in the center of the void, or more than 2.5 times the total ambient field strength, while dropping below 2 nT (<30%) in the rarefaction regions.

2.2. The 13 March 2013 Observation

Figure 2 shows an ARTEMIS P1 observation of extreme diamagnetic fields on 13 March 2013. In contrast to the first observation, the Moon was located in the solar wind at this time at [56.9, 19.8, 3.1] R_E GSE, Figure 2a. ARTEMIS P1 crossed the lunar wake diagonally from approximately 0.75 R_L downstream at the wake entrance to 2 R_L downstream at wake exit, Figure 2b, somewhat farther downstream than the 8 October 2011 observation, while P2 was far from the moon, Figure 2c. The ion and electron temperatures

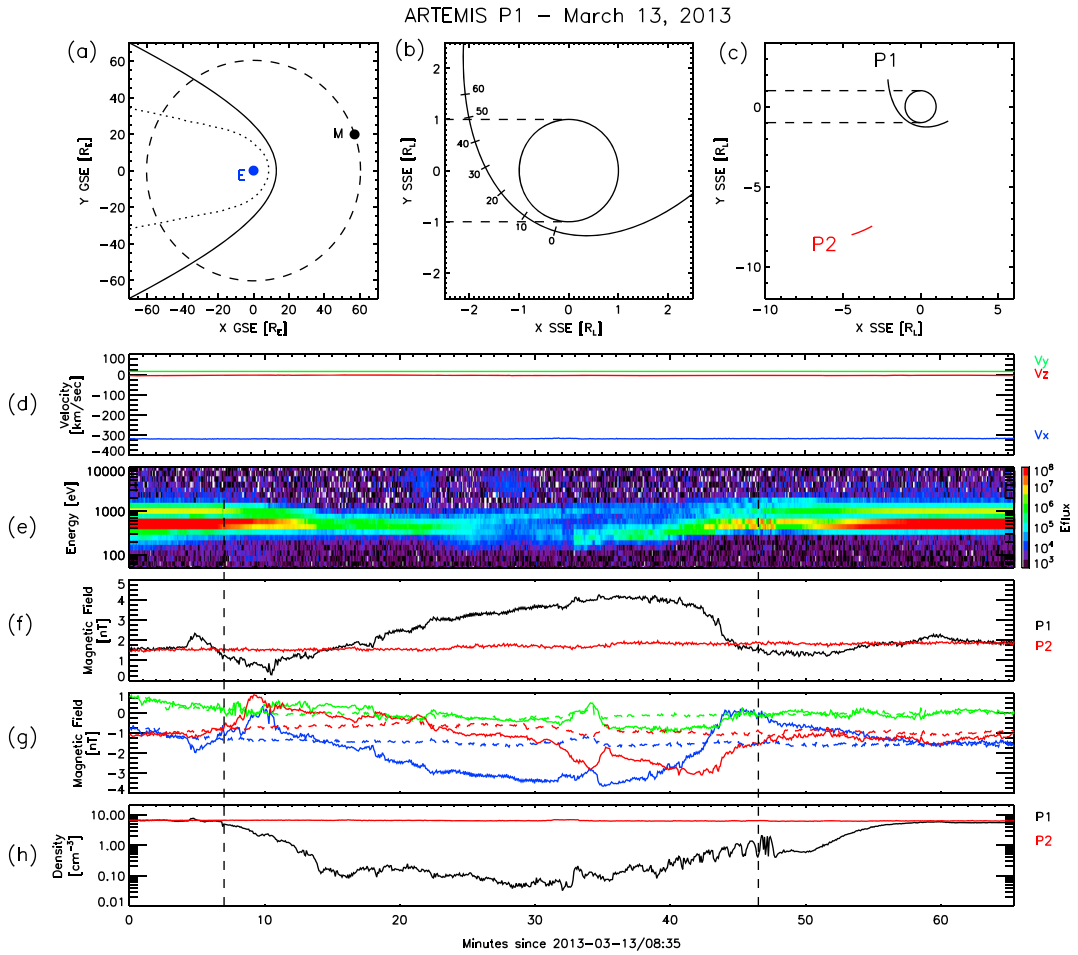

Figure 2. A time series of ARTEMIS P1 measurements on 13 March 2013 in the same format as Figure 1, measured in minutes since 13 March 2013/08:35.

were typical of the solar wind (10 and ≈4–6 eV, respectively); however, the magnetic field magnitude was significantly below typical solar wind values at only 1.6 nT. As summarized in Table 1, the low magnetic field strength during this time drove the electron and ion beta to 7.8 and ≈3.5–5, respectively, in total slightly higher than found in the previous observation in the terrestrial magnetosheath. The magnetic field magnitude across the wake, Figure 2f, has compressional features outside the optical boundary (approximately 5 and 60 min, respectively), rarefaction regions (7 to 15 and 44 to 56 min, respectively), and a strong diamagnetic field enhancement in the center of the wake (15 to 44 min). Inspecting the magnetic field components in Figure 2g shows that most features in the magnitude are driven by changes in the B_x and B_z components. At maximum, the magnetic field magnitude in the wake exceeds 4 nT, over 250% of the ambient field strength. The density in Figure 2h shows a 2 order-of-magnitude decrease through the central wake. We note that the oscillations in the density from approximately 43 to 48 min are unphysical due to angular undersampling of the cold ion beams penetrating into the wake [*McFadden et al.*, 2008; *Halekas et al.*, 2014]. Additionally, the two small bursts of high-energy ions at $t = 22$ and 28 min are terrestrial foreshock ions traveling sunward at fluxes too low to perturb the lunar wake.

The compressional features in the density and magnetic field magnitude on both sides of the wake at $t = 5$ and 60 min are most likely due to protons reflected off of crustal magnetic anomalies on the lunar dayside. The large crustal magnetic anomaly located in the South Pole/Aitken Basin region was near the subsolar point at this time and as previous observations have shown, reflects a significant portion of the incoming solar wind proton flux away from the lunar surface [*Lue et al.*, 2011]. A full analysis and discussion of the compressional features is beyond the scope of the current paper, but identified as a future study.

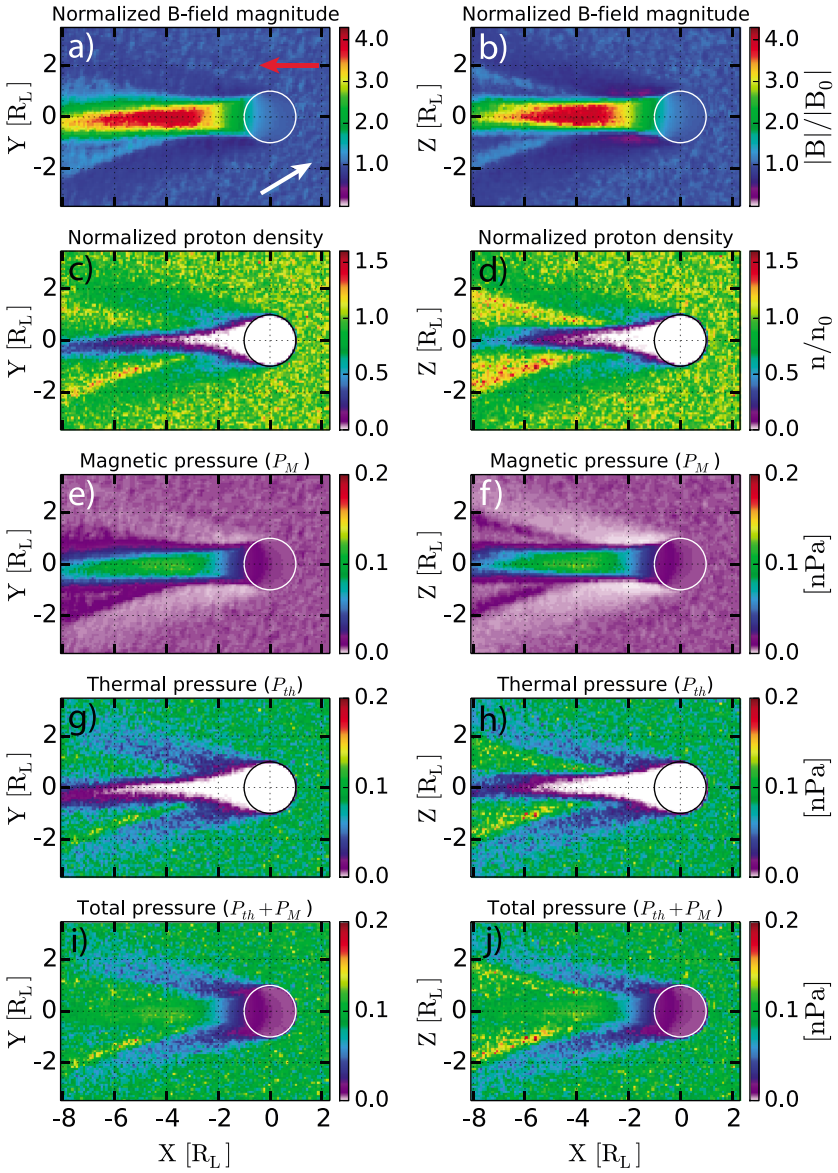

Figure 3. (a, b) Normalized magnetic field magnitude, (c, d) normalized proton density, (e, f) magnetic pressure (perpendicular), (g, h) particle pressure, and (i, j) total pressure obtained from the hybrid simulations of plasma interaction with the Moon. Upstream plasma parameters are listed in Table 1 (model), noting that we use the rotated frame appropriate for modeling as discussed in section 3. The arrows in Figure 3a indicate the plasma flow (red) and magnetic field (white) directions. Figures 3b, 3d, 3f, 3h, and 3j are in the plane $z = 0$ (viewed from $+z$), and Figures 3a, 3c, 3e, 3g, and 3i are in the plane $y = 0$ (viewed from $-y$).

3. Hybrid Modeling

In order to elucidate the global structure of the lunar wake during times of extreme diamagnetic fields, we have used a three-dimensional self-consistent hybrid plasma model to simulate the 8 October 2011 ARTEMIS observation shown in Figure 1. We chose this observation over the March 2013 observation as this event had steadier background magnetic fields, a more symmetric ARTEMIS trajectory through the wake, and no obvious effects of crustal magnetic fields and/or reflected protons as discussed above in section 2.2. We use the hybrid model described in *Holmström et al.* [2012] with modifications to the handling of particle removal at boundaries and vacuum regions as described in *Holmström* [2013]. In order to simplify the model-data comparison, we have first rotated the ARTEMIS data into a coordinate frame that eliminates both the off-axis solar wind velocity components and the out-of-ecliptic-plane components of the magnetic field at each individual time. In other words, we align the data coordinate frame at each time such that

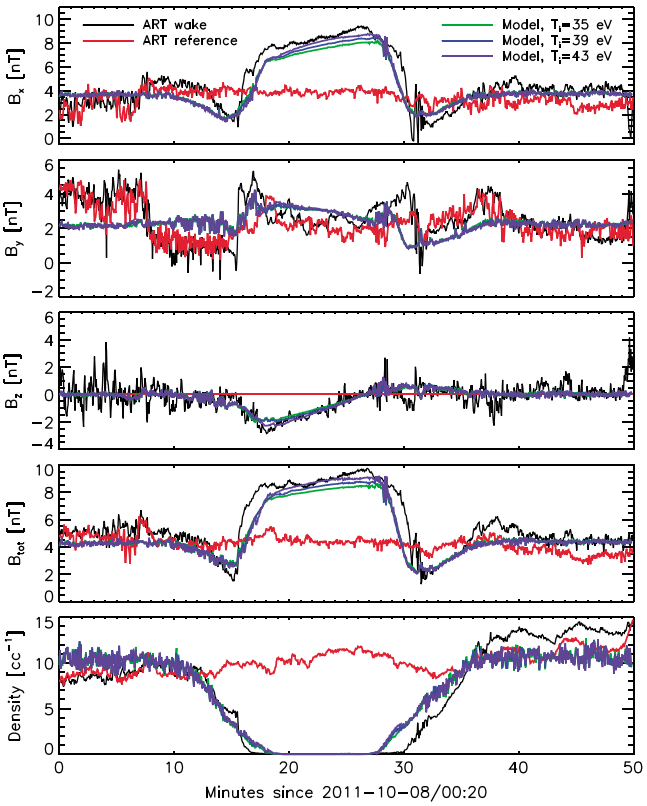

Figure 4. A comparison of ARTEMIS data and hybrid modeling results for the 8 October 2011 wake observations. Shown from top to bottom are the magnetic field components, magnetic field magnitude, and density, respectively. As discussed in section 3, the comparison is conducted in the rotated frame appropriate for modeling.

the solar wind flow velocity is completely and solely along the $-X$ axis while the magnetic field vectors are entirely in the X-Y plane. This rotation is also applied to the ARTEMIS trajectory across the wake, creating an effective trajectory used to interpolate through the model. For the October 2011 event, these rotations yielded an average magnetic field vector, [3.68, 2.23, 0.00] nT, and a flow velocity of 307 km/s during the wake crossing, summarized in Table 1. Due to the inherent uncertainty in determining the solar wind ion temperature from ARTEMIS, we ran three identical simulations while only varying the ion temperature at $T_i = 35, 39,$ and 43 eV. The simulation cell size was 150 km ($\approx$ 0.08 R_L) and the simulations were run until equilibrium was reached.

Figure 3 shows the normalized magnetic field magnitude, normalized proton density, and magnetic, particle, and total (magnetic plus particle) pressure in both the X-Y and X-Z planes with $T_i = 43$ eV for the October 2011 observation. Given the pressure gradient in the wake induced by the loss of solar wind particles, the plasma begins to refill the wake by compressing the ambient magnetic field in the perpendicular direction. This compression reaches its maximum at approximately 2.5–3 R_L downstream, where the diamagnetic field in the wake reaches over 4 times the ambient field strength. At this distance, the total plasma pressure has reached the ambient value ($\approx$ 0.13 nPa) and, at least within the optical wake, perpendicular pressure gradients cease to exist (rarefaction and recompression waves are evident propagating away outside the central wake). Given the relatively higher ion temperature during this observation, this compression happens somewhat faster compared to previous simulations with lower particle temperatures [*Wang et al.*, 2011; *Holmström et al.*, 2012; *Xie et al.*, 2012]. Farther downstream from this point, parallel motion is left as the dominant refill mechanism for the void, which slowly increases the density and decreases the diamagnetic field strength within the central void. This process is asymmetric due to the slightly tilted magnetic field geometry, and thus, the wake refills faster in X-Y plane from the $+Y$ flank than from the $-Y$ flank. Eventually, the wake will completely refill and return the diamagnetic field to its original undisturbed value; however, we note that for the high beta case presented here, the magnetic field in the void is still more than 3 times the ambient solar wind field strength at 8 R_L downstream.

Figure 4 shows the comparison of the rotated ARTEMIS data from both the reference and wake probes in red and black, respectively, along with the three model results using different ion temperatures interpolated along the effective ARTEMIS trajectory. Note that the coordinate system used for this comparison is the flow-aligned, planar-magnetic field system discussed above, and thus, the individual ARTEMIS vector components are rotated from those shown in Figure 1. In the rotated frame, the undisturbed ARTEMIS B_x field is nearly constant at approximately 3.7 nT, the B_y component has some variability at the 2–3 nT level but has an average value during the wake crossing of approximately 2.2 nT, and $B_z \equiv 0$ (by design). The wake probe (black) shows diamagnetic fields in all three components in this frame, mainly in the x component.

The ambient density increases somewhat over the period of the wake crossing in both probes, with a slightly larger increase in the wake probe, most likely due to small-scale structure in the magnetosheath. Traced along the effective ARTEMIS trajectory, the hybrid model succeeds in capturing the presence of strong diamagnetic fields in the lunar wake with corresponding deep depressions in the field outside the central cavity, with the $T_i = 43$ eV case matching the closest, specifically in the B_x and B_{total} components. The model does predict a narrower wake in both magnetic field and density, although, such a discrepancy is most likely caused by the finite cell size in the model, which at 150 km will tend to smear out subcell-sized variability. We anticipate that running the model with finer resolution may allow us to better capture such rapid spatial changes in the fields, being mindful of the increased computational requirements for such an exercise, which is beyond our current computational ability. Despite this discrepancy, the model successfully captures the B_x and B_z diamagnetic field enhancements while the B_y component does suffer some discrepancy, which we attribute to the more variable nature of the undisturbed ARTEMIS B_y component in the rotated frame. We also note the possible role that solar wind proton temperature anisotropy may play in contributing to the disagreement between the model and the data. ARTEMIS' ability to resolve both the parallel and perpendicular ion temperatures is limited in its current operating mode and any anisotropy may effect the magnitude of the field compression in the wake compared to the isotropic assumption used in the hybrid model.

Fatemi [2014] has derived an analytic relation between solar wind beta and the maximum diamagnetic field strength relative to the ambient field strength for parallel flow-IMF conditions as, $B_{\text{max}}/B_{\text{sw}} = \sqrt{1+\beta}$. The 2011-10-08 observation can be approximated as parallel and using parameters from Table 1, the analytic expression gives $B_{\text{max}}/B_{\text{sw}} \approx 3.4$–$3.6$, slightly lower than the maximum field ratio observed in the model of 4.2. For $\beta < 1$ conditions, the diamagnetic anomaly, $\Delta B = (B_{\text{max}} - B_{\text{sw}})/B_{\text{sw}}$, can be expressed using a Taylor expansion of the above analytic formula as $\Delta B \approx \beta/2$, recovering the linear relation noted in *Ogilvie and Ness* [1969]. A full understanding of the dependence between beta and diamagnetic fields must also take into account IMF-flow angle and downstream distance—an investigation for which the combination of the ARTEMIS data set and hybrid modeling is uniquely suited.

4. Conclusion

We have presented two ARTEMIS observations of extreme diamagnetic fields in the lunar wake, both under conditions with total plasma beta greater than 10. During such conditions, particle pressure dominates the total plasma pressure, and thus, when the Moon absorbs nearly the entire solar wind particle distribution, the ambient magnetic fields must significantly increase within the plasma void in order to attempt to restore the total plasma pressure. While previous observations have shown diamagnetic increases of at most 150% of the ambient magnetic field magnitude [*Ogilvie and Ness*, 1969; *Halekas et al.*, 2005; *Zhang et al.*, 2012], the observations presented here show increases of 230% and 250% and provide important end-member cases for testing theories and models of the dependence of lunar wake structure on ambient plasma parameters. Notably, the two ARTEMIS observations presented here, Figures 1 and 2, have distinctly different ambient plasma parameters with the exception of total plasma beta, reenforcing and extending the correlation between maximum diamagnetic field strength in the wake at approximately 1–2 R_L downstream and plasma beta found in *Ogilvie and Ness* [1969]. Indeed, reported observations of diamagnetic fields in the wakes of airless bodies throughout the solar system now span 3 orders of magnitude in ambient plasma beta, from outer planet moons such as Tethys and Rhea around Saturn where beta is as low as 0.03 [*Khurana et al.*, 2008; *Simon et al.*, 2012] to Earth's Moon, with total beta greater than 10 for the observations presented here.

Comparison of one of the observed extreme diamagnetic events with a plasma hybrid model has yielded a positive comparison along the ARTEMIS trajectory, with similar diamagnetic field components and magnitudes. Additionally, the simulations suggest that for this case, the maximum diamagnetic field increase throughout the entire lunar wake should occur for distances greater than three lunar radii downstream at a strength of approximately 18 nT, or an increase of 425% over the ambient field strength. Continued searches through and analysis of the extensive collection of ARTEMIS lunar wake crossings may yield observations of even greater diamagnetic field increases than are reported here as well as providing a database with which to statistically investigate the governing processes of both the lunar wake and the wakes of airless bodies throughout the solar system.

Acknowledgments
A.R.P, J.S.H, and G.T.D. gratefully acknowledge support from NASA's Solar System Exploration Research Virtual Institute (SSERVI). This publication is SSERVI contribution SSERVI-2014-093. The ARTEMIS mission is funded and operated under NASA grant NAS5-02099, and we specifically acknowledge J. P. McFadden for the use of ESA data and K.-H. Glassmeier, U. Auster, and W. Baumjohann for the use of FGM data provided under the lead of the Technical University of Braunschweig and with financial support through the German Ministry for Economy and Technology and the German Center for Aviation and Space (DLR) under contract 50 OC 0302. All ARTEMIS data necessary to reproduce this work are publicly available at http://artemis.ssl.berkeley.edu. The authors also acknowledge the International Space Science Institute (ISSI) for hosting a workshop series that in part inspired this work. The hybrid modeling was conducted using resources provided by the Swedish National Infrastructure for Computing (SNIC) at the High Performance Computing Center North (HPC2N), Umeå University, Sweden. The software used in this work was in part developed by the DOE NNSA-ASC OASCR Flash Center at the University of Chicago. The authors thank two reviewers for helpful and constructive comments.

The Editor thanks Hui Zhang and an anonymous reviewer for their assistance in evaluating this paper.

References

Angelopoulos, V. (2011), The ARTEMIS mission, *Space Sci. Rev.*, *165*, 3–25.

Colburn, D. S., R. G. Currie, J. D. Mihalov, and C. P. Sonett (1967), Diamagnetic solar-wind cavity discovered behind Moon, *Science*, *158* (3804), 1040–1042.

Fatemi, S. (2014), Kinetic modeling of the solar wind plasma interaction with the Moon, PhD thesis, Swedish Institute of Space Physics, Luleå Univ. of Technology, Luleå, Sweden.

Fatemi, S., M. Holmström, Y. Futaana, S. Barabash, and C. Lue (2013), The lunar wake current systems, *Geophys. Res. Lett.*, *40*, 17–21, doi:10.1029/2012GL054635.

Halekas, J. S., S. D. Bale, D. L. Mitchell, and R. P. Lin (2005), Electrons and magnetic fields in the lunar plasma wake, *J. Geophys. Res.*, *110*, A07222, doi:10.1029/2004JA010991.

Halekas, J. S., D. A. Brain, and M. Holmström (2014), The Moon's plasma wake, in *Magnetotails in the Solar System*, edited by A. Keiling, AGU, Washington, D. C.

Halekas, J. S., et al. (2011), First results from ARTEMIS, a new two-spacecraft lunar mission: Counter-streaming plasma populations in the lunar wake, *Space Sci. Rev.*, *165*, 93–107.

Holmström, M. (2013), Handling vacuum regions in a hybrid plasma solver, in *Numerical Modeling of Space Plasma Flows (ASTRONUM 2012)*, vol. 474, edited by N. V. Pogorelov, E. Audit, and G. P. Zank, pp. 202–207, Astronomical Society of the Pacific, San Francisco, Calif.

Holmström, M., S. Fatemi, Y. Futaana, and H. Nilsson (2012), The interaction between the Moon and the solar wind, *Earth Planets Space*, *64*, 237–245.

Kallio, E. (2005), Formation of the lunar wake in quasi-neutral hybrid model, *Geophys. Res. Lett.*, *32*, L06107, doi:10.1029/2004GL021989.

Khurana, K. K., C. T. Russell, and M. K. Dougherty (2008), Magnetic portraits of Tethys and Rhea, *Icarus*, *193*, 465–474.

Lue, C., Y. Futaana, S. Barabash, M. Wieser, M. Holmström, A. Bhardwaj, M. B. Dhanya, and P. Wurz (2011), Strong influence of lunar crustal fields on the solar wind flow, *Geophys. Res. Lett.*, *38*, L03202, doi:10.1029/2010GL046215.

McFadden, J. P., C. W. Carlson, D. Larson, J. Bonnell, F. Mozer, V. Angelopoulos, K.-H. Glassmeier, and U. Auster (2008), THEMIS ESA first science results and performance issues, *Space Sci. Rev.*, *141*, 477–508.

Ness, N. F., K. W. Behannon, H. E. Taylor, and Y. C. Whang (1968), Perturbations of the interplanetary magnetic field by the lunar wake, *J. Geophys. Res.*, *73*(11), 3421–3440.

Ogilvie, K. W., and N. F. Ness (1969), Dependence of the lunar wake on solar wind plasma characteristics, *J. Geophys. Res.*, *74*(16), 4123–4128.

Owen, C. J., R. P. Lepping, K. W. Ogilvie, J. A. Slavin, W. M. Farrell, and J. B. Byrnes (1996), The lunar wake at 6.8 R_L: WIND magnetic field observations, *Geophys. Res. Lett.*, *23*(10), 1263–1266.

Simon, S., H. Kriegel, J. Saur, A. Wennmacher, F. M. Neubauer, E. Roussos, U. Motschmann, and M. K. Dougherty (2012), Analysis of Cassini magnetic field observations over the poles of Rhea, *J. Geophys. Res.*, *117*, A07211, doi:10.1029/2012JA017747.

Trávníček, P., P. Hellinger, D. Schriver, and S. D. Bale (2005), Structure of the lunar wake: Two-dimensional global hybrid simulations, *Geophys. Res. Lett.*, *32*, L06102, doi:10.1029/2004GL022243.

Wang, Y.-C., J. Müller, W.-H. Ip, and U. Motschmann (2011), A 3D hybrid simulation study of the electromagnetic field distributions in the lunar wake, *Icarus*, *216*, 415–425.

Wiehle, S., et al. (2011), First lunar wake passage of ARTEMIS: Discrimination of wake effects and solar wind fluctuations by 3D hybrid simulations, *Planet. Space Sci.*, *59*, 661–671.

Xie, L., L. Li, Y. Zhang, and D. L. De Zeeuw (2012), Three-dimensional MHD simulation of the lunar wake, *Sci. China Earth Sci.*, *56*, 330–338.

Zhang, H., et al. (2012), Outward expansion of the lunar wake: ARTEMIS observations, *Geophys. Res. Lett.*, *39*, L18104, doi:10.1029/2012GL052839.